

Computer simulation of thromboexclusion of the complete aorta in the treatment of chronic type B aneurysm

Nenad Filipovic, Dalibor Nikolic, Igor Saveljic, Tijana Djukic, Oto Adjic, Pavle Kovacevic, Nada Cemerlic-Adjic & Lazar Velicki

To cite this article: Nenad Filipovic, Dalibor Nikolic, Igor Saveljic, Tijana Djukic, Oto Adjic, Pavle Kovacevic, Nada Cemerlic-Adjic & Lazar Velicki (2013) Computer simulation of thromboexclusion of the complete aorta in the treatment of chronic type B aneurysm, *Computer Aided Surgery*, 18:1-2, 1-9, DOI: [10.3109/10929088.2012.741145](https://doi.org/10.3109/10929088.2012.741145)

To link to this article: <https://doi.org/10.3109/10929088.2012.741145>



© 2013 Informa UK Ltd All rights reserved:
reproduction in whole or part not permitted



Published online: 26 Nov 2012.



Submit your article to this journal [↗](#)



Article views: 397



View related articles [↗](#)



Citing articles: 5 View citing articles [↗](#)

BIOMEDICAL PAPER

Computer simulation of thromboexclusion of the complete aorta in the treatment of chronic type B aneurysm

NENAD FILIPOVIC^{1,2,3}, DALIBOR NIKOLIC^{1,3}, IGOR SAVELJIC^{1,3},
TIJANA DJUKIC^{1,3}, OTO ADJIC⁴, PAVLE KOVACEVIC^{5,6}, NADA CEMERLIC-ADJIC^{5,6},
& LAZAR VELICKI^{5,6}

¹Faculty of Mechanical Engineering, University of Kragujevac, Kragujevac, Serbia; ²Molecular and Integrative Physiological Sciences, Harvard School of Public Health, Boston, Massachusetts; ³BioIRC, Research and Development Center for Bioengineering, Kragujevac, Serbia; ⁴Imaging Diagnostic Center, Institute of Oncology Vojvodina, Novi Sad, Serbia; ⁵Medical Faculty, University of Novi Sad, Novi Sad, Serbia; and ⁶Institute of Cardiovascular Diseases Vojvodina, Novi Sad, Serbia

(Received 14 June 2012; accepted 1 October 2012)

Abstract

The purpose of this computational study was to examine the hemodynamic parameters of the velocity fields, shear stress, pressure and drag force field in the complex aorta system, based on a case of type B aortic dissection. The extra-anatomic reconstruction of the complete aorta and bipolar exclusion of the aneurysm was investigated by computational fluid dynamics. Three different cases of the same patient were analyzed: the existing preoperative condition and two alternative surgical treatment options, cases A and B, involving different distal aorto-aortic anastomosis sites. The three-dimensional Navier-Stokes equations and the continuity equation were solved with an unsteady stabilized finite element method. The aorta and large tube graft geometries were reconstructed based on CT angiography images to generate a patient-specific 3D finite element mesh. The computed results showed velocity profiles with smaller intensity in the aorta than in the graft tube in the postoperative case. The shear stress distribution showed low zones around 0.5 Pa in the aneurysm part of the aorta for all three cases. Pressure distribution and, particularly, drag force had much higher values in the preoperative aneurysm zones (7.37 N) than postoperatively (2.45 N), which provides strong evidence of the hemodynamic and biomechanical benefits of this type of intervention in this specific patient. After assessing the outcome obtained with each of the two alternatives A and B, for which we found no significant difference, it was decided to use option A to treat the patient. In summary, computational studies could complement surgical preoperative risk assessment and provide significant insight into the benefits of different treatment alternatives.

Keywords: Chronic type B aortic aneurysm, extra-anatomic reconstruction, thromboexclusion, finite element modeling

Introduction

The aorta – the main conduit through which cardiac output is delivered to the systemic arterial bed – is continuously exposed to high pulsatile pressure and shear stress, making it susceptible to mechanical injury. An aortic dissection is a life-threatening condition arising from a tear in the inner layer of the aortic wall, allowing blood to flow through an unnatural passage within the aortic wall – a false

lumen [1]. The hemodynamic properties of blood flow through the false lumen, as well as the interplay in “dominance” between the false and true lumina, may have a significant impact on the outcome of surgery and survival [2]. Parallel blood flow through the false lumen may lead to a number of different scenarios, including the spread of a dissection to other peripheral arteries, aortic rupture, creation of a re-entry tear in the distal aorta, false lumen

thrombosis, true lumen occlusion, and development of post-dissection aneurysm. Determining the risk factors that may have a crucial role in aortic dissection onset and the development of complications has become an integrated multidisciplinary task oriented toward obtaining a thorough understanding of the pathogenesis and evolution of aortic dissection through computational studies.

Aortic dissections can be categorized based on the time from pain onset and anatomic location. With regard to anatomic distribution, aortic dissections are generally categorized according to the Stanford classification system as either type A aortic dissections (TAAD), occurring in the ascending aorta, or type B aortic dissections (TBAD), occurring in the descending aorta. Further subdivision into acute, subacute or chronic regimes is based on time scales of development.

Surgical treatment is almost always required in TAAD, whereas TBAD may be treated either surgically or medically (using anti-impulse therapy to reduce the impulse force $\Delta p/\Delta t$), depending on the clinical scenario and the extent of the dissection, and usually with a better prognosis. The goal of the treatment is to control the tear and prevent or treat complications. It is generally accepted that the optimal surgical treatment strategy for TBAD is inline reconstruction in total circulatory arrest with reattachment of all visceral branches [3, 4]. Other surgical approaches include extra-anatomic bypass, endovascular fenestration and, most recently, thoracic endovascular aortic repair (TEVAR).

The focus of this work is the assessment of the effect of surgical treatment of chronic TBAD using thromboexclusion and extra-anatomic bypass on the dynamic and geometric factors. Thromboexclusion implies an arterial reconstruction by an aorto-aortic bypass graft that is sutured in the non-dissected areas of the aorta and thereby avoids the dissected aorta and the need for extracorporeal circulation [5]. The main objective was to investigate how the flow field in the aorta was affected by flow condition, pressure and drag force, based on the case of a patient treated by extra-anatomic reconstruction and bipolar exclusion of the aneurysm.

The paper is organised as follows. The next section describes the basic finite element equations for blood flow analysis. Some of the results for shear stress, velocity, pressure, drag forces and streamlines for the preoperative situation and two different postoperative cases, A and B, are then presented, followed by a discussion and conclusions.

Methods

Generation of the geometric model

Using computer simulation, we attempted to analyze the case of a 55-year-old woman with a huge chronic post-dissection thoracoabdominal aneurysm with a maximal intrathoracic diameter of 13.5 cm and signs of intrathoracic imminent rupture with subparietal pleural hemorrhagic effusion [5].

In our clinic, end-to-side anastomosis between a large tube graft (26 mm) and the ascending aorta was performed. The left subclavian artery was prolonged with a 10-mm Dacron graft (Gelsoft™, Vascutek, a Terumo Company, Inchinnan, Renfrewshire, Scotland) and replanted to a new “mother graft”. The brachiocephalic artery was also replanted to the mother graft through the 10-mm Dacron prosthesis [5]. A schematic presentation of the aorta and graft system is shown in Figure 1, including the preoperative case and two possible postoperative alternatives. We distinguished two post-surgery cases (case A and case B) which represented two possible ways of treating the patient, including the influence on postoperative recovery. Case A was the treatment that was actually performed on this particular patient. An additional aim of this study was to investigate whether there was any difference between cases A and B.

A patient-specific geometric model of the thoracic aorta and its branches was created from 1-mm DICOM images of a CT angiography (CTA) examination acquired with a multi-detector-row CT scanner (Figure 2). Segmentation was performed using MIMICS software (Materialise NV, Leuven, Belgium), and the results expressed as a surface triangulation in stereolithography (STL) format. Several different regions of the thoracic aorta were included in the finite element mesh: the ascending aorta (AA), the aortic arch with the roots of the brachiocephalic trunk (BCT), the left common carotid artery (LCA) and left subclavian artery (LSA), and the descending aorta (DA), as well as the graft, the prosthesis, and the aortic aneurysm. Finite element meshes were generated using FEMAP software (Siemens PLM Software) for generation of a tetrahedral mesh for any 3D polyhedron in conjunction with our own software tools written in C++ for conversion of tetrahedral elements to 8-node brick elements.

A finite element mesh is created using a custom algorithm for cutting and semi-automatically connecting triangles in order to maintain a smooth shape for the model, as illustrated in Figure 3. A Laplacian smoothing technique was implemented in order to obtain a smooth surface mesh after cutting and connection [6]. Mesh independence

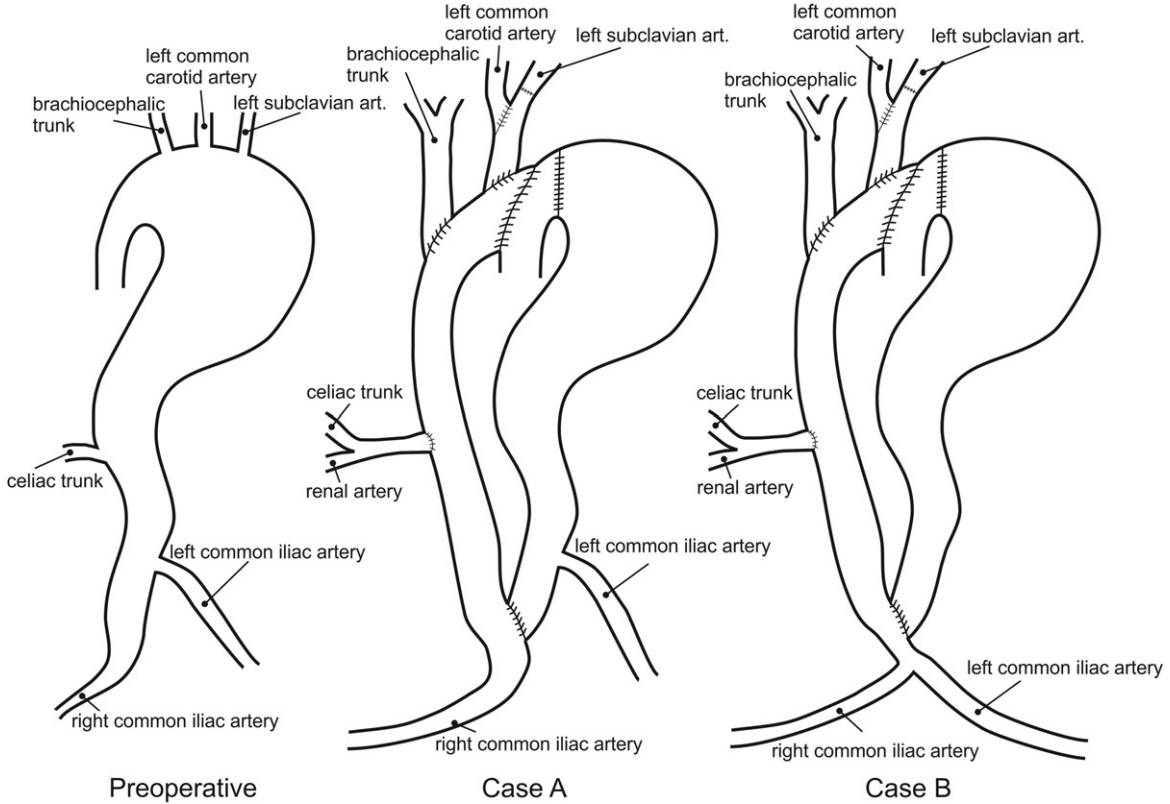


Figure 1. Schematic presentation of the preoperative case and two alternative postoperative cases (cases A and B) for extra-anatomic reconstruction and thromboexclusion in the patient.

analysis was performed using the results from two different mesh resolutions. Mesh independence was reached at 630 000 to 880 000 finite elements, with error of less than 1%.

Boundary conditions

The boundary conditions for flow were taken from a routine 2D MRI phase-contrast measurement of our patient in the preoperative condition, providing the pulsatile aortic flow conditions (Figure 4). The inlet aortic flow is prescribed at the root of the ascending aorta part, while at the three aorta branches, the brachiocephalic, common carotid and subclavian arteries, the patient pressure outlet is prescribed as measured from the systemic blood pressure.

A flat flow velocity profile is prescribed at the aortic inlet, which is justified by *in vivo* measurements using hot-film anemometry on various animal models [7]. The outlet of the descending aorta is represented by a traction-free boundary condition with uniform normal pressure, which is a good approximation for rigid wall models [8, 9].

Numerical calculations

Flow in the ascending aorta is a complex time-dependent 3D flow. In-house software was used for this complex time-dependent and fully 3D fluid flow. The code was validated using the analytical solution for shear stress and velocities through a 3D curved tube [10, 11] (www.bioirc.ac.rs). The 3D flow of a viscous incompressible fluid, as considered here, is governed by the Navier-Stokes equations and the continuity equation, which can be written as follows:

$$\rho \left(\frac{\partial v_i}{\partial t} + v_j \frac{\partial v_i}{\partial x_j} \right) = - \frac{\partial p}{\partial x_i} + \mu \left(\frac{\partial^2 v_i}{\partial x_j \partial x_j} + \frac{\partial^2 v_j}{\partial x_j \partial x_i} \right) \quad (1)$$

$$\frac{\partial v_i}{\partial x_i} = 0 \quad (2)$$

where v_i is the blood velocity in direction x_i , ρ is the fluid density, p is the pressure, μ is the dynamic viscosity; and summation is assumed on the repeated (dummy) indices, $i, j = 1, 2, 3$. The first equation represents the balance of linear momentum, while Equation (2) expresses the incompressibility condition.



Figure 2. Thromboexclusion of the aorta with extra-anatomic aortic bypass with reattached supra-aortic, visceral, and lower limb vessels.

Each waveform of the input aorta and the three branches was discretized into 400 uniformly spaced time steps. A penalty formulation was used in our solver [10].

The incremental-iterative form of the equations for time step Δt and equilibrium iteration i are as follows:

$$\begin{bmatrix} \frac{1}{\Delta t} \mathbf{M}_v + {}^{t+\Delta t} \mathbf{K}_{vv}^{(i-1)} + {}^{t+\Delta t} \mathbf{K}_{\mu v}^{(i-1)} + {}^{t+\Delta t} \mathbf{J}_{vv}^{(i-1)} & \mathbf{K}_{vp} \\ \mathbf{K}_{vp}^T & \mathbf{0} \end{bmatrix} \times \begin{Bmatrix} \Delta \mathbf{v}^{(i)} \\ \Delta \mathbf{p}^{(i)} \end{Bmatrix} = \begin{Bmatrix} {}^{t+\Delta t} \mathbf{F}_v^{(i-1)} \\ {}^{t+\Delta t} \mathbf{F}_p^{(i-1)} \end{Bmatrix} \quad (3)$$

The left upper index $t + \Delta t$ denotes that the quantities are evaluated at the end of a time step. The matrix \mathbf{M}_v is a mass matrix, \mathbf{K}_{vv} and \mathbf{J}_{vv} are convective matrices, $\mathbf{K}_{\mu v}$ is the viscous matrix, \mathbf{K}_{vp} is the pressure matrix, and \mathbf{F}_v and \mathbf{F}_p are forcing vectors. The pressure is eliminated at the element level through the static condensation. A parallel

version of the solver is used (www.bioirc.ac.rs), and for this purpose two cycles with 400 time steps per cycle took 14 hours on 64 processors with 2 GB RAM.

In addition to the velocity field, the wall shear stress computation is performed. The mean shear stress τ_{mean} within a time interval T is calculated as in reference [9]:

$$\tau_{mean} = \left| \frac{1}{T} \int_0^T t_s dt \right| \quad (4)$$

where t_s is the surface traction vector. Another scalar quantity is a time-averaged magnitude of the surface traction vector, calculated as

$$\tau_{mag} = \frac{1}{T} \int_0^T |t_s| dt \quad (5)$$

Results

Velocity profiles

The 3D velocity vector field is presented in Figure 5 under pulsatile flow condition at peak systolic flow. It can be seen that before the treatment higher velocities dominated in the ascending aorta as well as in the bottom part of the descending aorta. For both postoperative cases A and B the higher velocities are observed in the ascending aorta, graft tube and iliac arteries. The aneurysm lumen obviously has a very low velocity field or almost zero flow.

Pressure distribution for the cases before and after treatment is shown in Figure 6. The aneurysm part of the aorta dominated with higher pressure before treatment, which proves the hypothesis of possible rupture under the delicate preoperative conditions. Obviously, surgical intervention decreases blood pressure significantly in the aneurysm domain, which is a huge benefit for this particular intervention. It can be observed that, even with very low flow intensity in the aneurysm domain, there is still some pressure intensity.

Shear stress distribution for the cases before and after the treatment is presented in Figure 7. We observed slightly higher values for the shear stress in the preoperative case, but these were probably without any significant influence on the patient's preoperative condition.

What is very important in this computational study is the analysis of the drag forces from the blood flow domain. As higher blood pressure was measured in the patient, we presented results for the drag forces only for the peak systolic segment of the cardiac cycle (Figure 8). It appears that pressure presence in the aneurysm part of the aorta caused

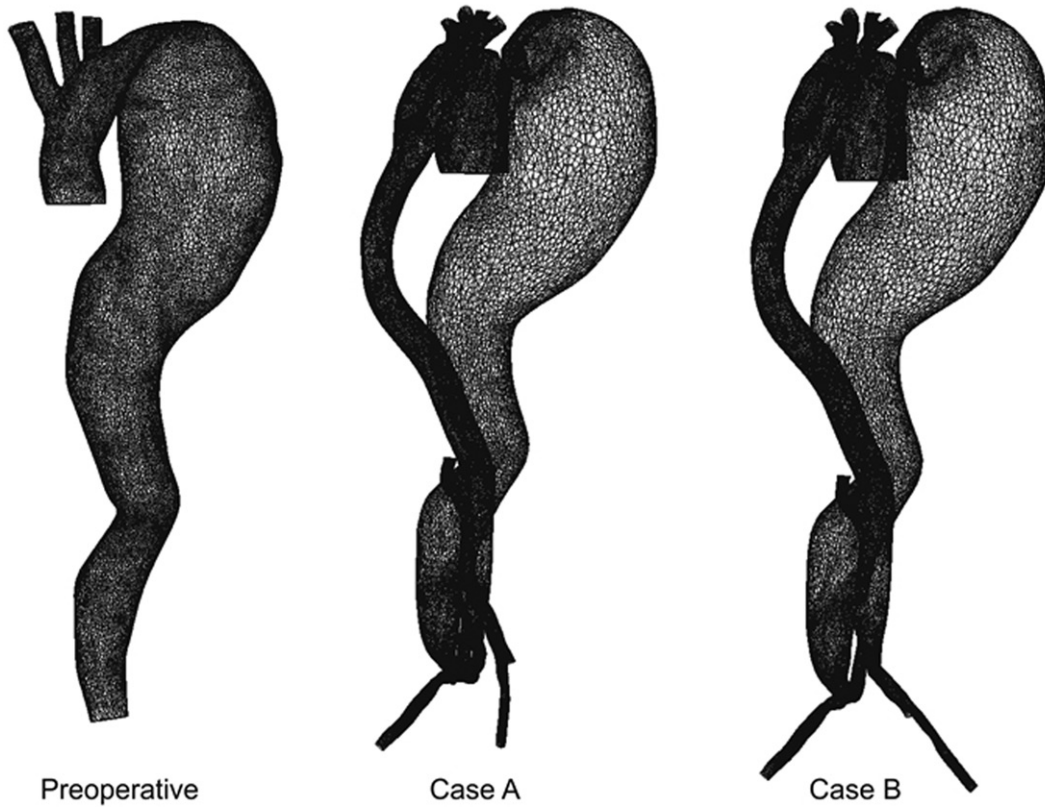


Figure 3. Finite element meshes for the preoperative case and the two postoperative cases A and B.

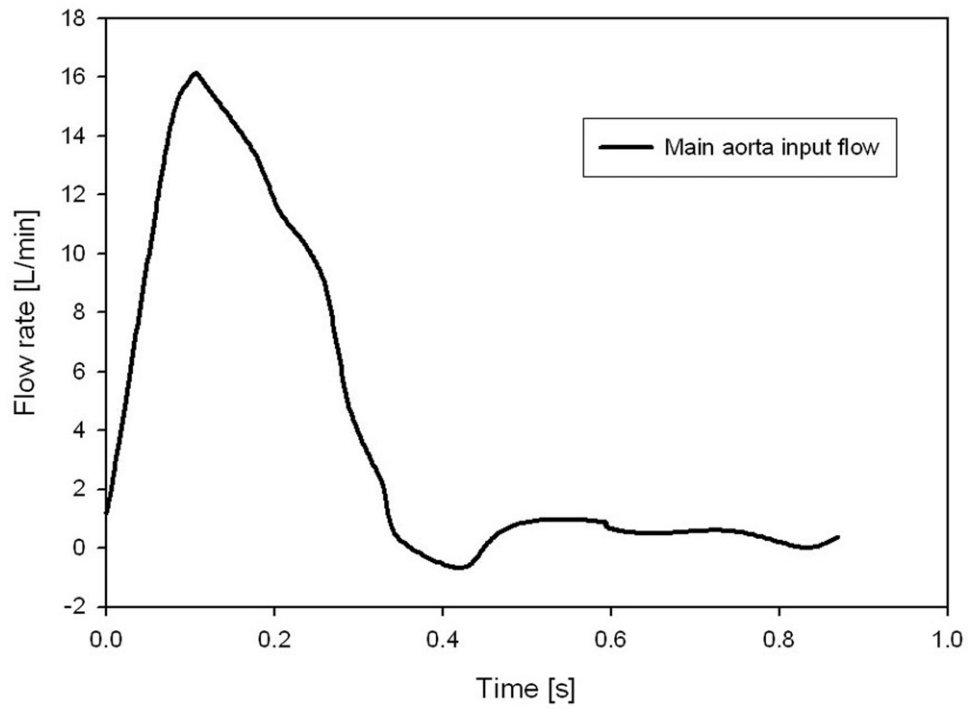


Figure 4. Input flow rate for the ascending aorta.

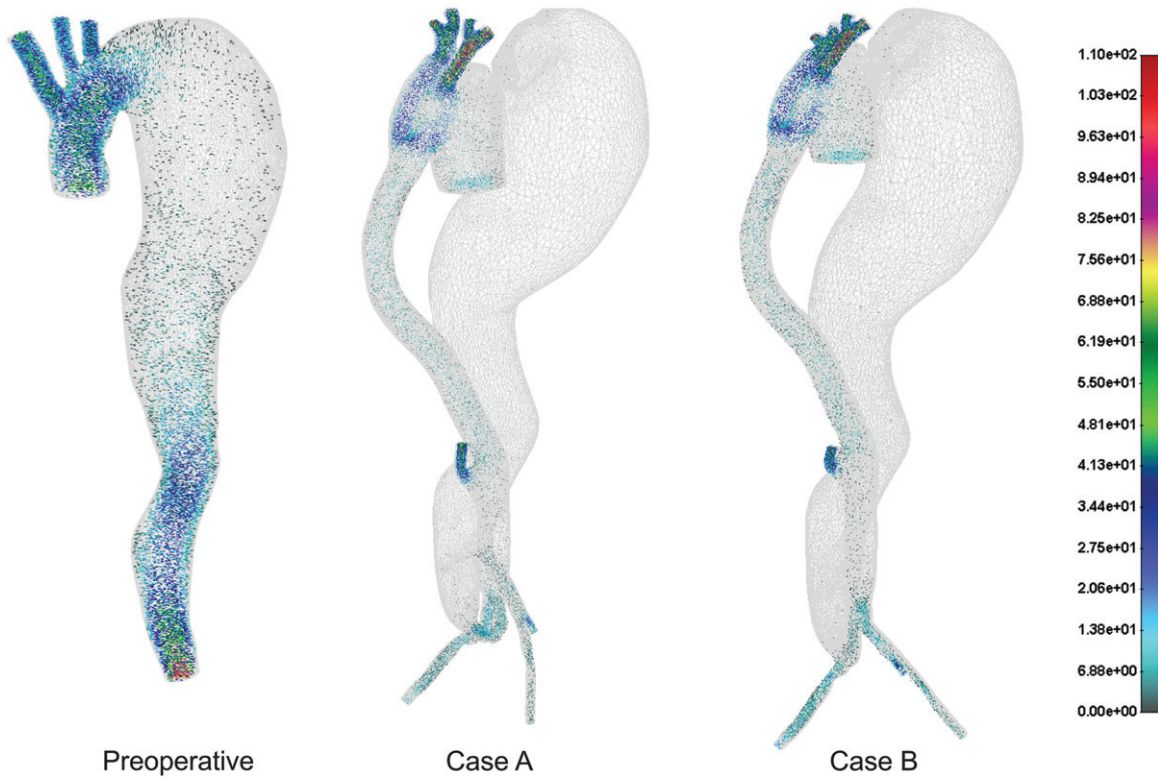


Figure 5. Velocity vector field for peak systolic flow within the thoracic aorta (units are cm).

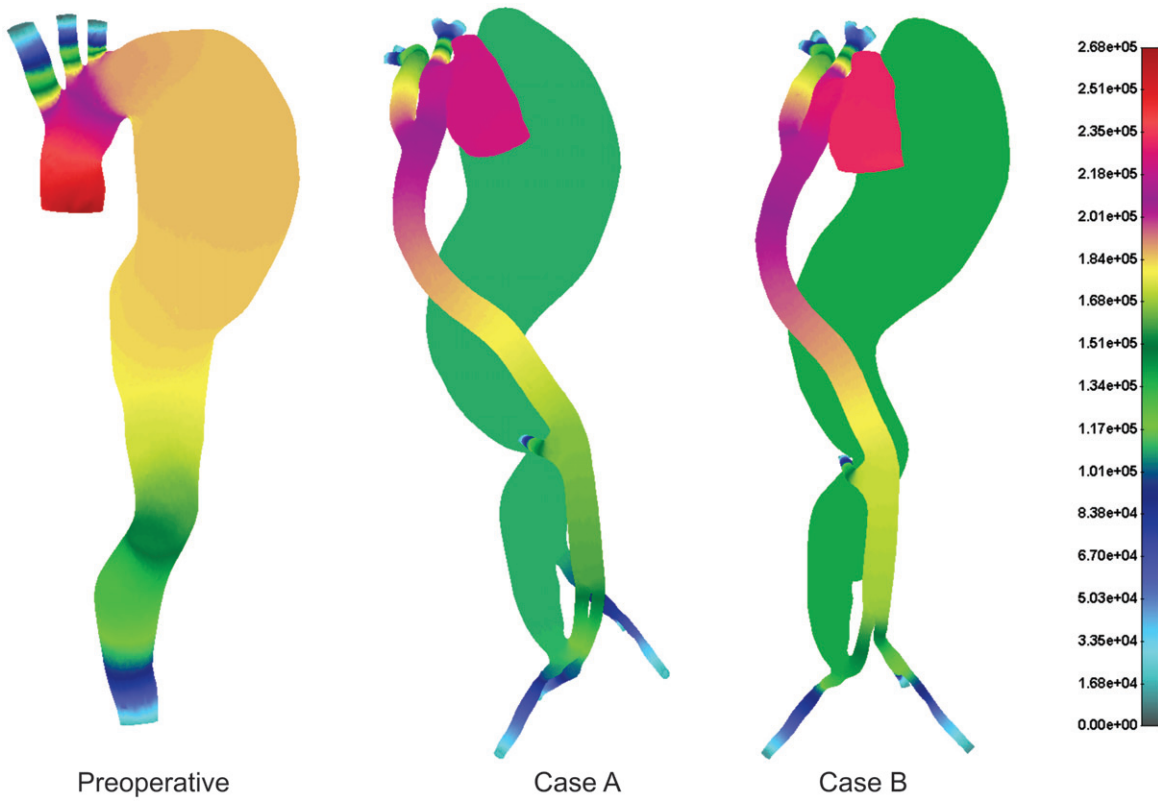


Figure 6. Pressure distribution for the cases before and after treatment.

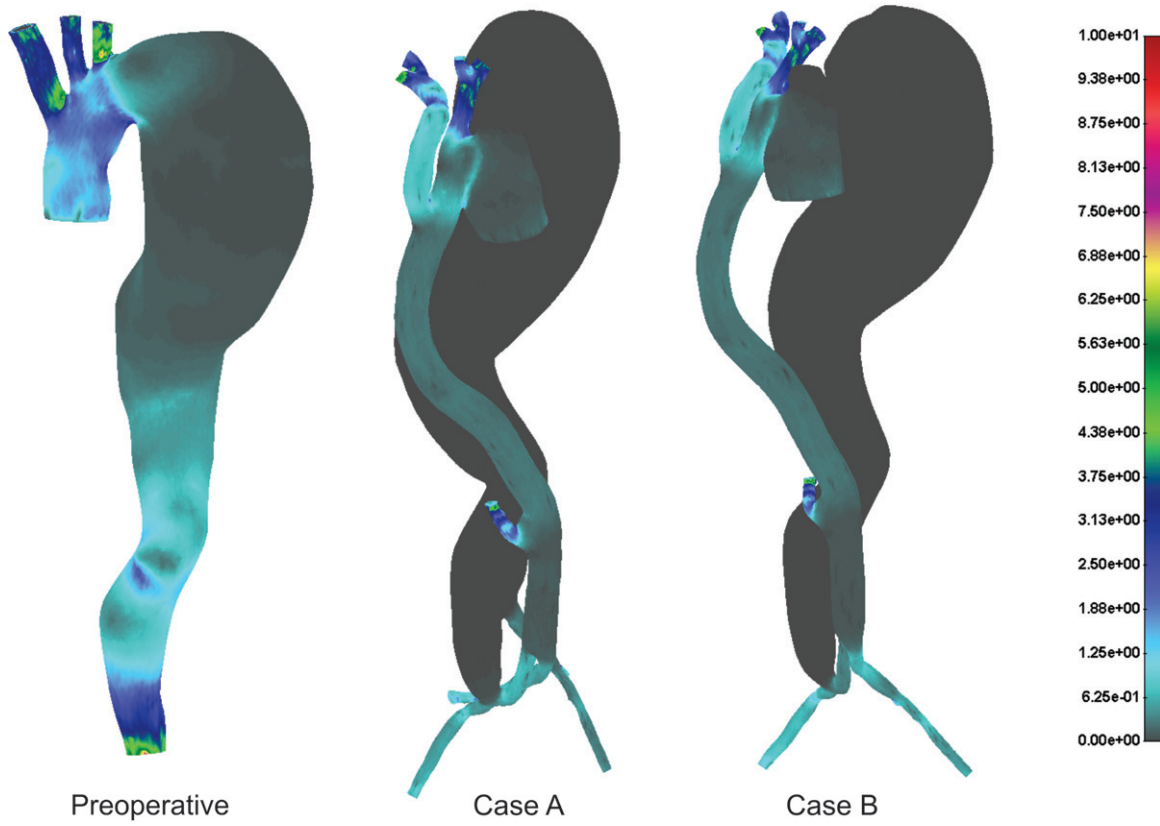


Figure 7. Shear stress distribution for the cases before and after treatment.

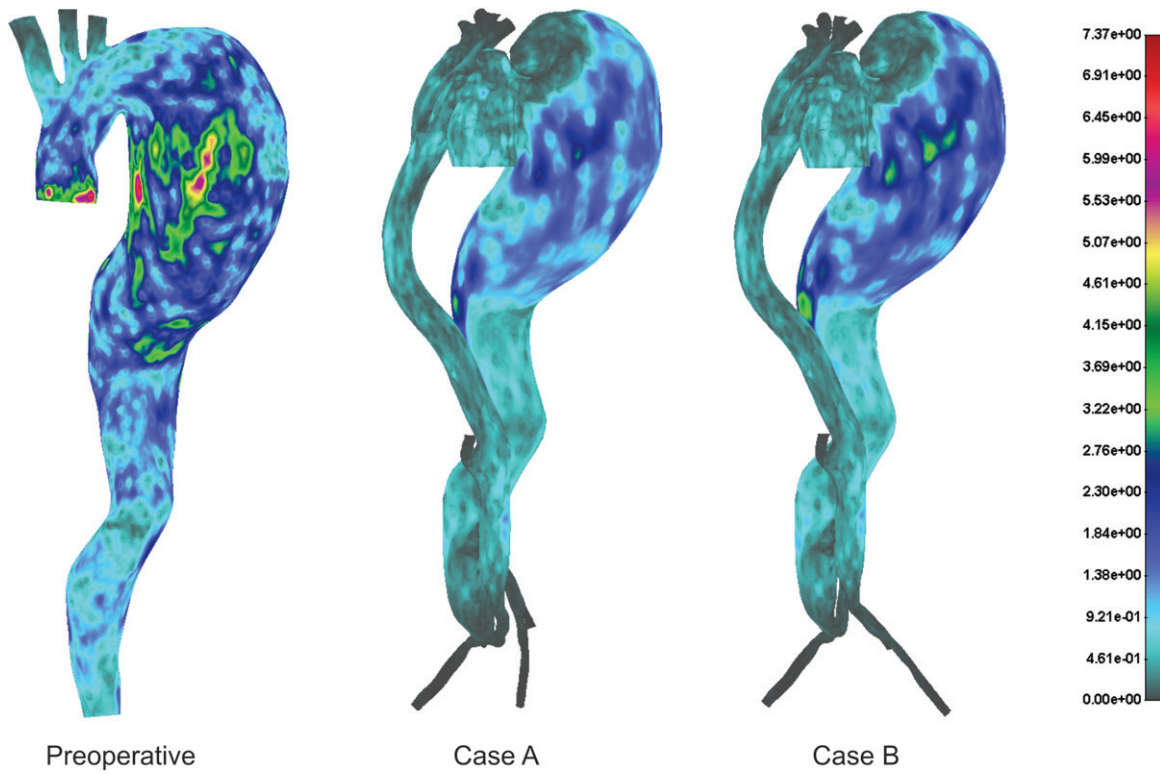


Figure 8. Drag force distribution for the preoperative case and the two alternative postoperative cases A and B.

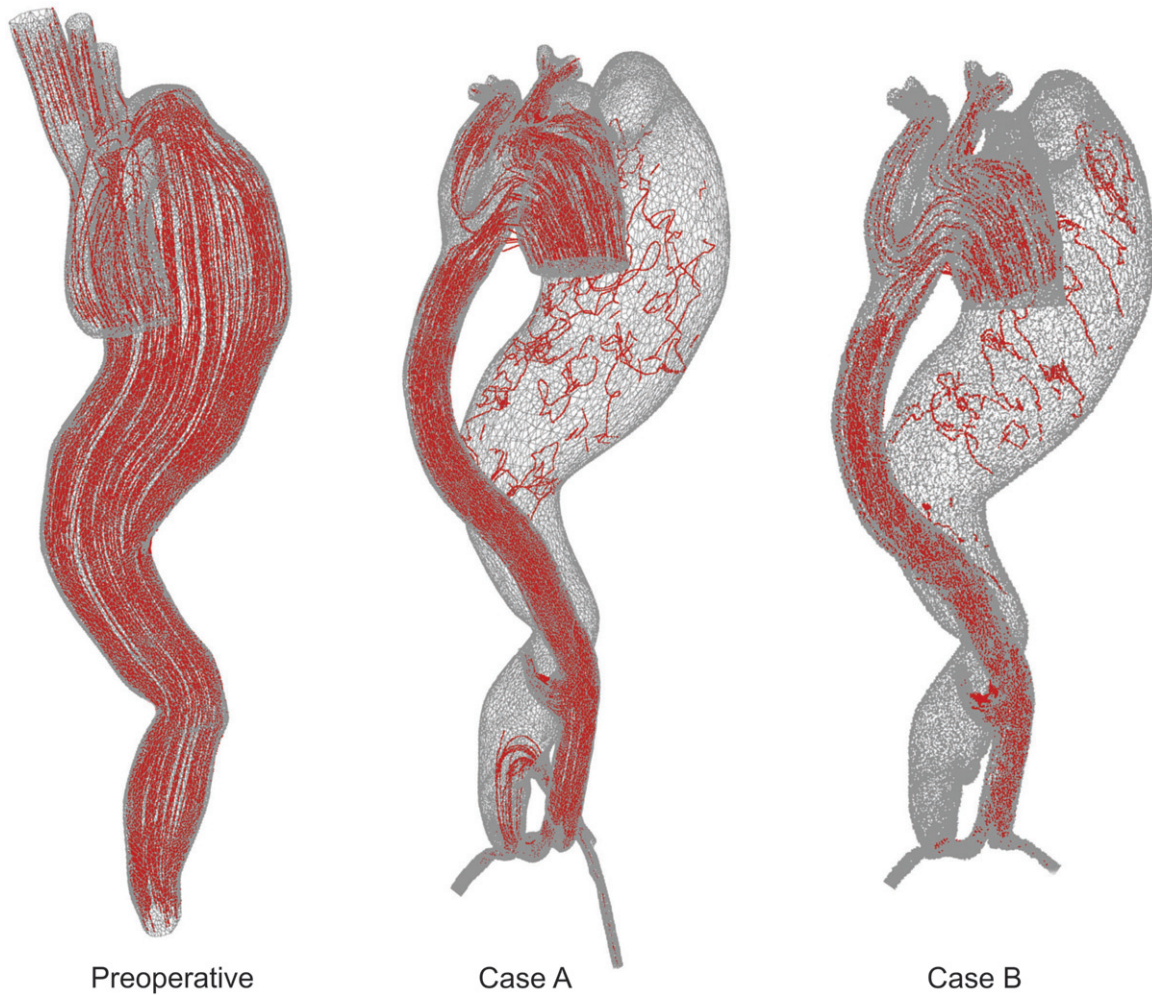


Figure 9. Streamline distribution for the preoperative case and the two alternative postoperative cases A and B.

the higher drag force in the preoperative case. This is direct evidence of the benefit to the patient of this operative treatment. Streamline distributions for the preoperative and postoperative cases A and B are shown in Figure 9. For the preoperative case there is a large streamline flow inside the aneurysm, while for cases A and B only some small recirculation zones are found, due to the very low flow intensity.

Discussion and conclusions

We performed computational fluid dynamics (CFD) simulation for the specific case of the treatment of a chronic type B aneurysm with extra-anatomic reconstruction of the complete aorta and thromboexclusion of the aneurysm. Three different computational models were investigated. Preoperative and two alternative postoperative cases, A and B, were analyzed by

computer simulation. The postoperative cases A and B differed in terms of the site of the distal aorto-aortic anastomosis and iliac artery starting position. Case A was actually implemented in this patient. An additional purpose of the computational study was to examine whether there was any difference between the two cases A and B. End-to-side anastomosis between a large tube graft and the ascending aorta, as well as replantation of the left subclavian and brachiocephalic arteries, was implemented.

Patient-specific geometries were derived from 3D CT angiography data, and physiologic blood flow values were obtained by 2D phase-contrast MRI. CFD analysis investigated velocity and pressure distribution, wall shear stress, drag force and streamlines.

Currently, the therapeutic effects on hemodynamic interactions with the vessel wall and an implanted medical device, e.g., an endovascular stent graft, can only be predicted prior to surgery by

simulation. Therefore, this study was intended to support the surgical decision-making process.

Our analysis of the numerical data revealed several findings. As expected, there were smaller velocity intensities in the postoperative cases. The lowest shear stress zone, around 0.5 Pa, occurred within the aneurysm in all the cases, which was not unexpected. Pressure distribution and, especially, drag force distribution give much more insight into the surgical outcome and probably predict some securing events for the patient.

Above all, the drag force was much higher in the preoperative case. The aneurysm part of the aorta post-treatment showed smaller drag force and the process of thromboexclusion almost stopped the blood flow in that part of the aorta. We identified the exact hemodynamic force values of around 7.37 N preoperatively and 2.45 N after treatment, which is still far from the rupture point of the surgical suture material [12]. No significant change was observed for the two different postoperative cases A and B in this computational biomechanical analysis, so case A was used to treat the patient.

Our studies had several limitations. First of all, the effect of aortic compliance was not considered in the present simulation. Scotti et al. [13] examined fluid-structure interaction in abdominal aortic aneurysm (AAA) and found that asymmetry and wall thickness have important roles with respect to risk of rupture. Mechanical stress inside the wall is the main criterion for ultimate rupture of AAA. Also, flow data were not taken from the same patient after treatment, and we do not have postoperative MRI data for validation of our simulation results. Finally, it is important to include wall mechanics and mass transport phenomena, which will be an objective of our future studies.

Declaration of interest: This work is supported partly by the Ministry of Education and Science in Serbia, with projects III41007,

ON174028 and FP7ICT-2007-2-5.3 (224297) ARTreat project.

References

- Juang D, Braverman AC, Eagle K. Cardiology patient pages. Aortic dissection. *Circulation* 2008;118(14):e507–e510.
- Karmonik C, Bismuth J, Davies MG, Shah DJ, Younes HK, Lumsden AB. A computational fluid dynamics study pre- and post-stent graft placement in an acute type B aortic dissection. *Vasc Endovascular Surg* 2011;45(2):157–164.
- Elefteriades JA. Natural history of thoracic aortic aneurysms: indications for surgery, and surgical versus nonsurgical risks. *Ann Thorac Surg* 2002;74(5):S1877–S1880.
- Svensson LG, Kouchoukos NT, Miller DC, Bavaria JE, Coselli JS, Curi MA, Eggebrecht H, Elefteriades JA, Erbel R, Gleason TG, et al. Expert consensus document on the treatment of descending thoracic aortic disease using endovascular stent-grafts. *Ann Thorac Surg* 2008;85(1 Suppl):S1–S41.
- Kovacevic P, Velicki L, Mojasevic R, Kieffer E. Thromboexclusion of the complete aorta in the treatment of chronic type B aneurysm. *Ann Vasc Surg* 2012 Feb;26(2):278–279.
- Pinkall U, Polthier K. Computing discrete minimal surfaces and their conjugates. *Experim Math* 1993;1:15–36.
- Nerem RM. Vascular fluid mechanics, the arterial wall, and atherosclerosis. *J Biomech Eng* 1992;114:274–282.
- Shahcheraghi N, Dwyer HA, Cheer AY, Barakat AI, Rutaganira T. Unsteady and three-dimensional simulation of blood flow in the human aortic arch. *J Biomech Eng* 2002;124:378–387.
- Taylor CA, Hughes TJR, Zarins CK. Finite element modeling of blood flow in arteries. *Comput Meths Appl Mech Eng* 1998;158:155–196.
- Filipovic N, Mijailovic S, Tsuda A, Kojic M. An implicit algorithm within the arbitrary Lagrangian-Eulerian formulation for solving incompressible fluid flow with large boundary motions. *Comp Meth Appl Mech Eng* 2006;195:6347–6361.
- Kojic M, Filipovic N, Stojanovic B, Kojic N. *Computer Modeling in Bioengineering: Theoretical Background, Examples and Software*. Chichester, England: John Wiley and Sons; 2008.
- Dobrin PB, Gosselin C, Kang S, Mrkvicka R. Effect of pulsatile pressure on the breaking strength and movement of Prolene sutures. *J Vasc Surg* 1997;29:1029–1035.
- Scotti CM, Shkolnik AD, Muluk SC, Finol EA. Fluid-structure interaction in abdominal aortic aneurysms: effects of asymmetry and wall thickness. *Biomed Eng Online* 2005;4:64.